Experimental studies of the Self-Centering Sliding Hinge Joint

H.H. Khoo, G.C. Clifton & J.W. Butterworth

Department of Civil Engineering, University of Auckland, Auckland.

G.A. MacRae

Department of Civil Engineering, University of Canterbury, Christchurch.

2012 NZSEE Conference

ABSTRACT: The Sliding Hinge Joint (SHJ) is a low damage connection that rotates inelastically with minimal damage through sliding of Asymmetric Friction Connections (AFC) in the bottom flange and web bolt groups. When this occurs the joint loses elastic strength and stiffness as the bolts in the AFCs lose tension. Furthermore, the SHJ does not have a recentering mechanism and thus does not always recenter. The self-centering SHJ (SCSHJ) was proposed which incorporates friction damping ring spings (RSs) as a self-centering component. This paper presents experimental studies on 6 full-scale subassembly joints. The joint moment capacities were developed with a combination of AFCs and RSs, and designed as a percentage of capacity generated by the RSs (P_{RS}). The joints produced stable and repeatable hysteretic behaviour, with minimal damage to the floor slab. The joints with just RSs exhibited the ideal flag-shaped self-centering hysteretic behaviour. The SCSHJ had a combination of the SHJ and RS behaviours, with improved self-centering characteristics as the P_{RS} increased. No loading rate effects were observed on the joint response. The SHJ had a 25% reduction in stable sliding capacity under a near fault pulse action due to increased demand on the bolts.

1 INTRODUCTION

The Sliding Hinge Joint (SHJ) is a low damage connection used in steel moment resisting frames (MRF). It was developed by Clifton (2005) as an alternative to traditional welded connections. It rotates inelastically with minimal damage to the joint while isolating the floor slab. This is achieved through sliding in Asymmetric Friction Connections (AFCs) to allow joint rotation. The AFC is a friction connection that decouples moment frame strength and stiffness and confines inelastic demand to the bolts. They are designed to be rigid under working load and serviceability limit state (SLS) conditions, and slide under ultimate limit state (ULS) events. Further developments were undertaken by MacRae et. al (2010) to establish the AFC dependable friction force, and the effects of aluminium and mild steel shims compared to brass shims tested by Clifton (2005). Mild steel shims were recommended and have since been used in construction. Khoo et. al (2012) tested the AFC with shims of different hardnesses, recommending the use of low alloy abrasion resistant steel shims. On-going research on implementing the AFC in other seismic resistant systems is currently underway (Kahn & Clifton 2011; Chanchi Golondrino et. al 2012).

The SHJ has benefits over welded connections which include (1) decoupling of moment frame strength and stiffness which enables larger beam sizes without imposing high overstrength demands on the columns, (2) confining inelastic demand to the bolts which is easily replaced following an earthquake, (3) improved seismic-dynamic recentering ability, (4) economically cheaper. The SHJ inelastic rotation is nevertheless associated with a loss of elastic strength and stiffness due to losses in clamping force as the bolts are subjected to additional inelastic action during sliding. Furthermore, the SHJ does not always return the frames to their pre-earthquake position, as the joint does not have a self-centering mechanism.

Khoo et. al (2011) proposed the self-centering version of the SHJ (SCSHJ) with enhanced recentering properties and reduced elastic strength and stiffness losses. It combines the behaviour of the SHJ with the self-centering behaviour of friction damping ring springs (RSs) manufactured by Ringfeder,

Germany (Ringfeder Gmbh 2008). The springs contribute to the joint moment capacity and provide a recentering force to return the joint to its original position. The joint properties can be altered by varying the percentage of moment capacity contributed by the RSs (P_{RS}), as described in Section 2.2.

Experimental studies on joint subassemblies representing an interior connection were undertaken at both quasi-static and seismic-dynamic rates of loading. The joints were designed with different P_{RS} levels. This paper presents the results of 6 tests, and provides answers to the following questions:

1. How do the SHJ and ring springs behave?
2. How does the SCSHJ behave?
3. Is the SHJ performance loading rate dependent?
4. How does the SHJ perform under a near fault pulse action?

2 SELF-CENTERING SLIDING HINGE JOINT

2.1 *Joint description*

The SCSHJ is briefly described, with more details found in Khoo et. al (2011). Figure 1 shows a schematic drawing of the SCSHJ layout and RS configuration. The beam is connected to the column through the top flange plate which acts as the point of rotation. AFCs are installed in the bottom flange and web bolt groups. Figure 2a shows the idealised moment-rotational behaviour of the SHJ, which is determined by the AFC sliding characteristics.

The RS assembly consists of a cage which guides the spring to prevent buckling, and a threaded bar, nuts and endplates to transfer the load from the beams into the column. The assembly results in a dual-direction acting RS similar to that proposed by Filiatrault et. al (2000), which is then bolted to the bottom flange of the beam. The theoretical moment rotational behaviour of the RS contribution is shown in Figure 2b, which exhibits the ideal flag-shape self-centering hysteretic behaviour. Figure 2c shows the combined AFC and RS contributions in the SCSHJ. Note that it does not reflect the flag-shaped hysteretic behaviour of other self-centering systems which aim to develop static recentering properties. The objective of the SCSHJ is to improve seismic-dynamic recentering properties to a dependable level, which considers winding down effects of the structure following an earthquake (MacRae 1994). The SCSHJ has several benefits compared to the current SHJ namely: (1) the number of bolts in the AFC can be reduced, (2) energy stored in the spring contributes to joint re-centering upon load removal or reversal, and (3) loss in joint elastic strength due to bolt tension losses in the AFC can be compensated by spring pre-compression.

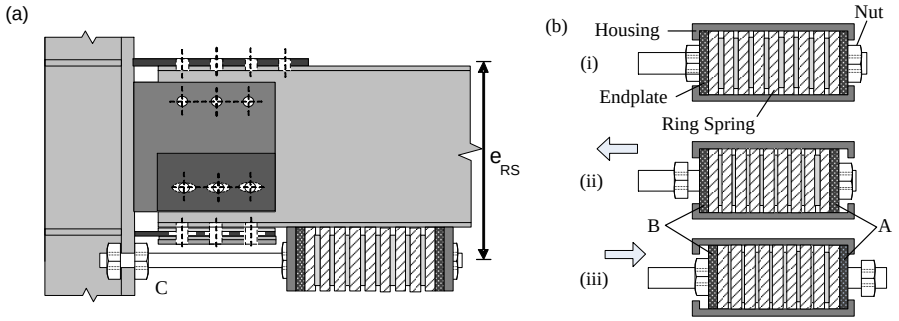

Figure 1: (a) SCSHJ layout and (b) ring spring layout (modified from Khoo et. al (2011))

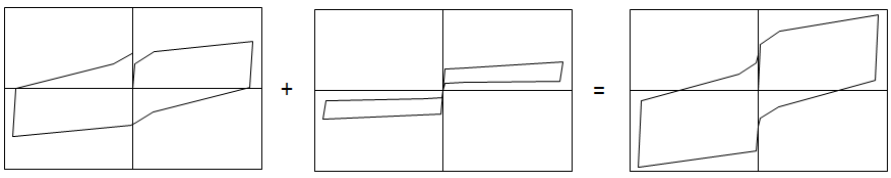

(a) (b) (c)

Figure 2: Idealised moment rotational behaviour (a) SHJ, (b) RS contribution and (c) SCSHJ (modified from Khoo (2011))

2.2 *Simplified analysis*

The flexural behaviour of the SCSHJ is a function of the sliding friction resistance in the AFCs, the force in the RS, and the respective lever arms to the point of rotation. It can be written as:

$$M_{SCSHJ} = M_{SHJ} + M_{RS} \quad (1)$$

$$M_{SHJ} = n_{wbb} V_{ss} e_{wb} + n_{bfb} V_{ss} d_b \quad (2)$$

$$M_{RS} = F_p e_{RS} \quad (3)$$

$$P_{RS} = \frac{M_{RS}}{M_{SCSHJ}} \times 100 \quad (4)$$

where M_{SCSHJ} = SCSHJ moment; M_{SHJ} = AFC moment contribution; M_{RS} = RS moment contribution; n_{wbb} = number of bolts in the bottom web AFC; n_{bfb} = number of bolts in the bottom flange AFC; e_{wb} = bottom web AFC lever arm (as shown in Fig. 1a); V_{ss} = sliding shear resistance per bolt; n_{bfb} = number of bolts in the beam bottom flange AFC; d_b = beam depth; F_p = RS pre-compression; e_{RS} = RS lever am (as shown in Fig. 1a); P_{RS} = percentage of moment capacity contributed by the RS.

These equations do not take into account secondary effects such the influence of the floor slab and deformation of the flange plates during rotation that increase the joint strength and stiffness (MacRae, Clifton et al. 2010).

3 **TEST DESCRIPTION**

3.1 *Test setup*

The test setup (Figure 3) simulated an internal connection in a MRF. It was based on the 8th floor of the 10 storey Te Puni Village building in Wellington, New Zealand (Gledhill, Sidwell et al. 2008). The test setup assumed the column mid-height and beam mid-span are points of inflection. The column was pinned at the bottom to allow rotation, with an actuator providing the load at the top. The beam ends were pinned to allow rotation and horizontal movement and prevent vertical movement. Table 1 gives component details and dimensions. All plates were mild steel, except the shims which were abrasion resistant plate with a specified hardness of 370 – 430 HB in the Brinell scale. The top flange plate had 10 M24 bolts with 26 mm diameter holes. The top and bottom web bolt groups were each three M16 bolts with 18 mm diameter holes. The bottom flange plate and web plate bottom bolt group had 55 mm slotted holes to allow sliding. All bolts were proof loaded using the turn of nut method.

Table 1. Test component details

Component	**Details/Dimensions**
Column	460 UB 76.6
Beams	360 UB 57
Top flange plates	515 mm × 200 mm × 20 mm
Web plates	285 mm × 305 mm × 12 mm
Web cap plates	250 mm × 100 mm × 16 mm
Bottom flange plates	335 mm × 155 mm × 12 mm
Bottom flange cap plates	175 mm × 155 mm × 16 mm
Inner web shims	285 mm × 250 mm × 6 mm
Outer web shims	250 mm × 100 mm × 6 mm
Upper bottom flange shims	195 mm × 280 mm × 6 mm
Lower bottom flange shims	195 mm × 175 mm × 6 mm

The column stiffener configuration (Figure 3b) allowed the RS bar to be connected to the column flange. A semi-circle hole was cut through the column web, with a semi-circular stiffener welded to the column. The stiffener was a 168.3 mm outside diameter, 14.27 mm thick tube to ASTM A106B with a specified yield and tensile strengths of 241 MPa and 414 MPa. It was 190 mm long to extend over the length of the column flange. The column flange had a 168 mm × 190 mm × 20 mm mild steel plate to prevent yield line failure of the flange. This was welded to the column and the tube with a square weld. A 38 mm diameter hole was then drilled through the column flange and stiffener. The column had a 10 mm thick doubler plate welded to the web, and 12 mm thick top and bottom continuity plates. The semi-circular stiffened hole in the column web was expensive, but allowed the use of one RS assembly per side. The cost saving from one RS assembly per side compensated for the cost of the column panel zone fabrication to accommodate the RS bar passing through the column web centreline. Note the horizontal stiffener in the column web situated in the middle of the panel zone region was present to allow an alternative self centering mechanism to be tested on this joint. That mechanism proposed the use of shape memory allow bars but problems with their manufacture and conditioning prior to testing ruled out their use.

A steel deck concrete slab was placed on the test assembly. The deck was Comflor 60 (Comflor 2008) installed perpendicular to the beams and cantilevering 500 mm out each side from the beam centreline. The slab was 125 mm thick and connected to the beams through six 19 mm diameter shear studs, stopping at a distance of $1.5d_b$ from the column face in accordance with standard practice. The concrete had a 28 day strength of 27.4 MPa. The slab reinforcement was 147/10 (665 equivalent), which is a 300 mm × 300 mm grid with 7.5 mm diameter wires with yield strength of 500 MPa.

Figure 3: Left to right: Test setup and column stiffener

3.2 *Test specimens*

The details of the 6 specimens are given in Table 2. Specimens SHJ and SHJ_NF were the standard SHJ, specimen RSJ only had the RSs, and the other specimens were SCSHJs with both AFCs and RSs. The RS was Type 12400, 40 elements long, and precompressed to 56.7% of its capacity. This corresponded to a theoretical capacity of 200 kN, stiffness of 1.92 kN/mm, and precompression of 113.5 kN. The number of bolts in the AFCs was then altered to vary the P_{RS}.

Table 2. Test matrix

Specimen	n_{wbb}	n_{bfp}	M_{SHJ} (kNm)	M_{RS} (kNm)	M_{SCSHJ} (kNm)	P_{RS} (%)
SHJ	3	4	123	0	123	0
SHJ_NF	3	4	123	0	123	0
P_{RS}_40.2	0	4	76.6	51.5	128.1	40.2
P_{RS}_40.2_Dy	0	4	76.6	51.5	128.1	40.2
P_{RS}_52.6	3	0	46.4	51.5	97.9	52.6
RSJ	0	0	0	51.5	51.5	100

The loading regime adopted was recommended by the SAC Joint Venture (2000) for steel MRF connection subassembly tests, which consisted of symmetric cycles of drift (δ). The regime was six

cycles of δ = 0.375%, 0.5%, and 0.75%, four cycles of δ = 1% and two cycles of δ = 1.5%, 2% and 3% at quasi-static rates of loading. The regime was applied at seismic rates of loading to P_{RS}_40.2_Dy by assuming a period of 1.5 s at δ = 2%, with the other δ periods scaled to reflect the same displacement rate at the top of the column. SHJ_NF was tested to the SAC Joint Venture (2000) near-fault recommendations, which incorporates a pulse cycle of δ = 6%. This regime was applied twice dynamically. The first was scaled to a maximum δ of 4.5% which is the limit of design joint rotation where the bolts hit the end of the slotted hole, followed by the same regime scaled to δ = 6%. In practice, the maximum δ achieved was 5.3% due to limitations of the testing facility.

4 TEST RESULTS AND DISCUSSION

The experimental results are summarised in Table 3. $M_{s,exp}$ is the stable sliding state moment, taken at zero displacement in the final cycle of loading for the SHJ specimen, and at the first instance when the moment-rotation curve reaches a plateau for the other specimens. This is because the RS theoretically has no contribution at zero displacement. The joint rotations (Θ_r) were determined through measuring the displacement of the beam bottom flange relative to the column face. The $M_{s,exp}/M_{s,the}$ ratio gives an indication of the joint overstrength factor, δ_m is the maximum drift and Θ_p is the maximum rotation. The recentering properties are evaluated in terms of the residual drift (δ_r), which is defined as the drift when the load is slowly reduced to zero from the maximum δ, and H_f which is the final actuator load when the column is brought back to the plumb position from maximum δ. They give an indication of the static recentering ability as the closer they are to zero, the better the performance. These values from δ = 2.0% is also presented. The behaviour of specimens SHJ and RSJ isolates the contribution of the AFC and RSs and is discussed first, followed by the SCSHJ specimens.

Table 3: Summary of test results.

Specimen	$M_{s,exp}$ (kNm)	$M_{s,exp}/M_{s,the}$	δ_m (%)	Θ_p (mrad)	H_f** (kN)	δ_r** (%)
SHJ	167.8	1.36	3.04	27.2	74.4 (50)	2.0 (1.2)
SHJ_NF	138.0	1.12	5.37(-3.79)*	43.7	-	-
PRS_40.2	157.7	1.23	3.03	27.8	53.6 (28.3)	1.51(1.2)
PRS_40.2_Dy	164.8	1.29	2.87	25.8	58.4 (25)	1.48 (1.3)
PRS_52.6	110.0	1.12	3.07	30.8	16.1 (25.0)	1.14 (0.8)
RSJ	57.5	1.12	3.09	30.4	8.4	0.36

* First application of regime in bracket

** Values from 2% drift in brackets

4.1 *SHJ and RSJ behaviour*

Figure 4a and b presents the joint moment-rotational (M-Θ_r) behaviour of specimens SHJ and RSJ respectively. The SHJ results were comparable to tests undertaken by Clifton (2005) and MacRae et. al. (2010). The joints remained essentially rigid till sliding commenced at approximately δ = 0.75%, corresponding to a Θ_r of approximately 1 mrad (milliradian). The curves were effectively bilinear and did not exhibit the theoretical two stage increase in resistance due to the bolts rotating and gradually taking up the frictional resistance which smear the double slip effect (MacRae et. al 2010). The resistance at load reversal was near zero, and increased as it was pushed in the other direction, giving the joint a "pinched" hysteretic curved. The $M_{s,exp}$ was 167.8 kNm, which is the moment at the final cycle of maximum rotation. The SHJ does not display static recentering properties as shown by the δ_r = 2.0% and H_f = 74.4 kN. From δ = 2.0%, the values were 1.2% and 50 kN respectively.

RSJ represent joints where the moment capacity is developed by the RS alone. The joint developed stable, ideal flag-shaped self-centering hysteretic behaviour (Figure 4b). The initial elastic stiffness was 18.4 kNm/rad and a definite yield moment indicated the point the RS started to compress. Inelastic

rotation commenced at a beam bottom flange deflection of 1.1 mm relative to the column, corresponding to a Θ_r of 3.1 mrad. Once the joints were in the inelastic range, the RS assembly performed as expected, compressing the springs during both positive and negative joint rotations. The inelastic stiffness was reasonably constant up to a rotation of 20 mrad. The self-centering ability of the joint is clearly shown by the δ_r and H_f values of 0.36% and 8.4 kN respectively.

A key difference in performance of the RSJ was the low elastic stiffness compared to the SHJ, due to the lack of pretension in the bar connecting the column and RSs. The stiffness was therefore dependent on the bar and nuts which had considerable flexibility and deformation in the threads. This is difficult to quantify given the variability in snug tight installation of the bolts. It was proposed that the RS pre-compression would compensate for any elastic strength loss in the SHJ due to the loss of bolt tension in the AFCs. However under the current configuration, the ring spring component does not have a high elastic stiffness due to the flexibility of the bar and deformation in the threads. This could potentially be reduced by using a shorter bar if the bottom flange plate and AFCs were removed, or by using a larger diameter bar, which reduces the column net cross-sectional area which may have consequences on the column capacity. There would nevertheless be a certain degree of flexibility due the lack of any pretension in the bar.

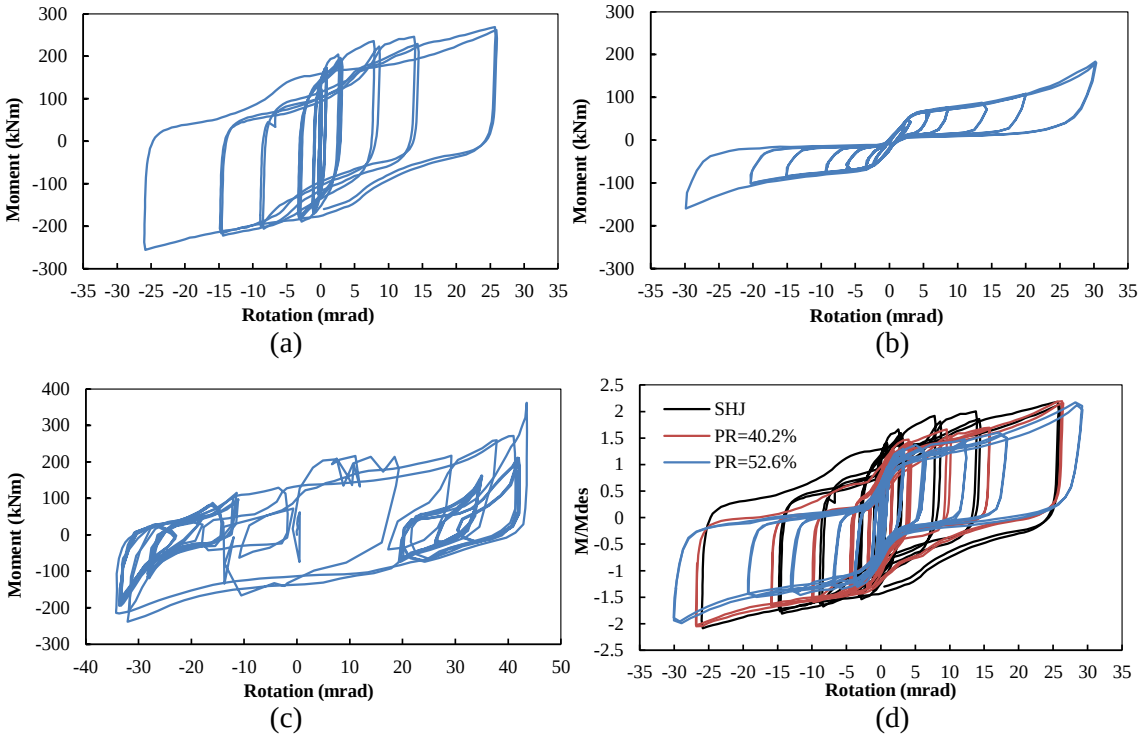

Figure 4: M-Θ_r for (a) SHJ, (b) RSJ, (c) SHJ_NF, and (d) Comparison of SCSHJ behaviour (moment normalised by design moment)

4.2 *SCSHJ behaviour*

The other specimens were designed to test the combination of AFC and RSs in the SCSHJ. Their M-Θ behaviour displays a combination of the AFC and RS characteristics as shown in Figure 4d. The SCSHJs behaved as expected, with the hysteresis curves getting closer to the ideal self-centering flag shaped curve of the RSJ as the P_{RS} increased. The recentering ability is shown by the reducing H_f and δ_r. The effects of the RSs can also be seen in the more pronounced pinched hysteretic curves.

Specimens P_{RS}_40.2 and P_{RS}_40.2_Dy were identical, with near identical response indicating there is no significant difference between the quasi-static and seismic-dynamic response of the joint. The H_f values were 53.6 kN and 58.4 kN, with the δr 1.51% and 1.48%. As such only P_{RS}_40.2 is shown in the figure. P_{RS}_52.6 had a larger P_{RS}, and therefore a higher recentering capability. The H_f and δ_r were 16.1 kN and 1.14% at 3% drift.

SHJ_NF was undertaken to test the SHJ under a near fault pulse action. The joint capacity was lower than that of the SHJ. The $M_{s,exp}$ was taken as the moment at the last cycle as it passed through the zero position. The initially lower strength is due to the lower friction levels as the sliding surfaces have yet to undergo "breaking-in", which can be 28% lower than the strength at stable sliding (Khoo, Clifton et al. 2012). This then increases as breaking-in occurs. However the extreme deformation caused the bolts to hit the end of the slotted hole, which resulted in a higher level of bolt tension loss due to greater inelastic deformation. This is seen as the spike in the positive direction of Figure 4c. There was nevertheless no excessive loss in strength, with the $M_{s,exp}$ at 75% of the expected strength.

4.3 *Post-yield behaviour*

The post-yield behaviour and stiffness is dependent on secondary elements and RS stiffness. The secondary elements effects are due to the rotational behaviour of the joint about the top flange plate. This causes prying of the flange plates during rotation (MacRae et. al 2010). The web plate and bolts are also contributing factors due to the rotation of the web plate about the beam, in contrast to the longitudinal directional sliding of the bottom flange plate. This adds extra demand on the top and bottom web bolts. The bottom web bolt impact marks indicate substantial vertical displacement during joint rotation. The web plate showed localised crushing on the horizontal sides of the slotted hole whereas the marks on the bottom flange AFC bolts indicate impact with the shims in the direction of sliding. These secondary effects are captured in the model previously developed (Clifton 2005) in Ruaumoko (Carr 2007).

The deformation of the slab was visually observed as the sides on either column faces rose and fell during rotation. The pattern and extent of slab damage is illustrated in Figure 5a, which shows slab cracking at various levels of δ. As the same slab was used for all specimens, the behaviour described is the response in the first test. A hairline crack first developed at the column flange interface at δ = 0.5%. As the column drifts increased, more cracks developed parallel to the column flange. The cracks at the column face eventually opened to around 1-2 mm during positive rotation at δ = 3% (Figure 5b). All other cracks remain hairline. There was crushing of the concrete around the column flanges at δ = 3.0% (Figure 5c). There was little change to the cracks away from the column in subsequent tests, but there was cumulative damage around the column with further crushing in the concrete. This slab behaviour is consistent with the stable and repeatable joint behaviour described in previous sections. The SHJ effectively isolated the floor slab and minimised any joint-slab interaction.

Figure 5: Left to right: Pattern of slab cracking, column face at 3% drift and cracking at column base

5 **FUTURE WORK**

The SCSHJs performed as expected with the recentering properties of the joint improving with increasing P_{RS}. The maximum P_{RS} of 52.3% was insufficient to develop static recentering properties. This was nevertheless not the objective of the SCSHJ, which is to improve the seismic-dynamic self-centering properties of the joint. Increasing the P_{RS} would increase the cost of the system and limit its implementation. The structure in reality would also be subjected to dynamic and winding-down effects. This will be the subject of future studies, which would include determining the effects of different P_{RS} on the seismic-dynamic recentering capability of the frame through dynamic inelastic time history analysis. Additionally, the RSs may not have to be installed at every joint. The option of installing the springs at selected levels, or particular joints will also be studied analytically.

6 CONCLUSIONS

1. The SHJ produced stable and repeatable hysteretic behaviour, and minimal damage to the floor slab. The RSJs exhibit the ideal flag-shaped self-centering hysteretic behaviour.
2. The SCSHJ had a combination of the SHJ and RSJ behaviours, with improved self-centering characteristics as the P_{RS} increased.
3. There is no difference in the response between specimens loaded quasi-statically and specimens loaded seismic-dynamically.
4. The SHJ had a 25% reduction in capacity under a near fault pulse action. This was due to increased demand on the AFC bolts, which decreases the frictional capacity of the joint.

7 ACKNOWLEDGEMENT

The authors would like to thank the New Zealand Earthquake Commission (EQC) for funding the test rig and specimens, and Composite Floor Decks Ltd for sponsoring materials and labour in the installation of the floor slab. All opinions expressed in this paper are those of the authors and do not necessarily represent those of the sponsor.

REFERENCES:

Carr, A. 2007. Ruaumoko. Department of Civil Engineering. University of Canterbury, Christchurch, New Zealand.

Chanchi Golondrino J., MacRae, G.A., Chase J.G., Rodgers, G.W., Mora Munoz, A., Clifton, G.C. 2012. Design considerations for braced frames with asymmetrical friction connections - AFC. *Proceedings of the 7th International Conference on Behaviour of Steel Structures in Seismic Areas, Santiago, Chile, 9-11 January 2012.*

Clifton, G.C. 2005. Semi-rigid joints for moment-resisting steel framed seismic-resisting systems. Department of Civil and Environmental Engineering. Auckland, University of Auckland.

Comflor. 2008. Comflor 60 Composite Floor Decking. Auckland, New Zealand.

Filiatrault, A., Tremblay, R., Kar, R. 2000. Performance Evaluation of Friction Spring Seismic Damper. *Journal of Structural Engineering* 126(4): 491-499.

Gledhill, S. M., Sidwell, G. K., Bell, D. 2008. The Damage Avoidance Design of tall steel frame buildings - Fairlie Terrace Student Accommodation Project, Victoria University of Wellington. *Proceedings of the 2008 New Zealand Society for Earthquake Engineerings: Engineering and Earthquake Resilient New Zealand. Taupo.*

Khan, M.J., C. Clifton. 2011. Proposed development of a damage resisting eccentrically braced frame with rotational active links. *Bulletin of New Zealand Society of Earthquake Engineering* 44(2): 99-107.

Khoo, H. H., C. Clifton, J.W. Butterworth, G.A. MacRae, G. Ferguson. 2012. Influence of steel shim hardness on the Sliding Hinge Joint performance. *Journal of constructional steel research* 72(0):119-129.

Khoo, H. H., C. Clifton, J.W. Butterworth, G.A. MacRae, C.D Mathieson. 2011. Development of the self-centering Sliding Hinge Joint. *Ninth Pacific Conference of Earthquake Engineering*. Auckland, New Zealand.

MacRae, G.A. 1997. P-D Effects on Single-Degree-of-Freedom Structures in Earthquakes. *Earthquake Spectra* 10(3): 539-568.

MacRae, G.A, Clifton, C., MacKinven, H., Mago, N., Butterworth, J., Pampanin, S. 2010. The Sliding Hinge Joint Moment Connection. *Bulletin of New Zealand Society of Earthquake Engineering* 43(3): 202-212

Ringfeder Gmbh. 2008. Damping Technology. Krefeld, Germany.

SAC Joint Venture. 2000. Recommended design criteria for new steel moment frame structures. Rep. No. FEMA-350, for the Federal Emergency Management Agency. Washington, D.C.